

Fluorescence Microtomography: External Mapping of Elements Inside Biological Samples

Christian G. Schroer^a, Johannes Tümmler^a, Til Florian Günzler^a,
Bruno Lengeler^a, Walter H. Schröder^b, Arnd J. Kuhn^b,
Alexandre S. Simionovici^c, Anatoly Snigirev^c, Irina Snigireva^c

^aII. Physikalisches Institut, Aachen University of Technology,
D-52056 Aachen, Germany

^bIBI 1, Forschungszentrum Jülich, D-52425 Jülich, Germany

^cEuropean Synchrotron Radiation Facility (ESRF), B.P. 220,
F-38043 Grenoble CEDEX, France

ABSTRACT

X-ray fluorescence element microtomography (XFEMT) allows to determine the element specific inner structure of a sample with resolutions in the micron range. It has a wide range of applications in many disciplines and is ideally suited for investigating element distributions inside of biological bulk samples at a cellular level with minimal sample preparation. The high intensity hard x-ray microbeam required for this scanning technique is produced using parabolic compound refractive lenses at a third generation undulator source. The sample is scanned through the microbeam in both translation and rotation and the fluorescence radiation created in the sample is recorded by an energy dispersive detector. From this data, the element distribution on a virtual section through the sample is recovered by tomographic techniques. The excitation of the fluorescence by monochromatic x-rays yields a high signal to background ratio and a low detection limit. As an example, we have investigated the distribution of physiologically relevant ions on a virtual section through a freeze dried root of the mahogany plant (*Swietenia macrophylla*). Absorption of the fluorescence radiation inside the sample has to be taken into account in tomographic reconstruction and ultimately limits the size of the sample that can be investigated. A self-consistent reconstruction technique not requiring the explicit knowledge of the absorption inside the sample has been developed. Further developments of the technique are discussed.

Keywords: Fluorescence tomography, element mapping, x-ray microbeam, compound refractive lenses

1. INTRODUCTION

For element analysis microbeam techniques with different probes (x-rays, electrons, ions) have become indispensable tools in many disciplines, e. g., material science, physics, chemistry, environmental science, and bio-medicine. The high sensitivity and low detection limits of microprobes with

Correspondence: C. G. Schroer. Email: schroer@physik.rwth-aachen.de

monochromatic hard x-rays at third generation synchrotron sources are of particular interest in the life and environmental sciences, as often the concentrations of the elements of interest are very low. Rapid advances in the fabrication of high quality focusing optics steadily improve the quality of hard x-ray microbeams and the number of beam time proposals to microprobe beamlines is growing quickly.

In conventional microprobe experiments, a thin slice or a surface of a specimen is scanned by the microbeam, requiring to prepare the sample in such a way as to bring the regions of interest to the surface. For biological specimen, this type of sample preparation is often very difficult if not impossible to achieve, since the elements of interest are typically highly diffusible in a complex and delicate matrix. To avoid shifting the element distributions, the samples are often shock frozen and cryo-sectioned, a procedure that is particularly difficult for plant samples. An external method that allows to measure distributions *inside* a specimen is therefore preferable for these samples or for samples that are too precious to be destroyed.

X-ray fluorescence element microtomography (XFEMT) is an external method that can be efficiently implemented at third generation synchrotron sources using compound refractive lenses. It allows to image the element distribution on a virtual section through the sample with a resolution in the micron range. Due to the detection of the fluorescence signal excited by monochromatic x-rays, the concentrations of the elements under consideration can be very low.

The sample investigated in this article is a shock frozen and freeze dried root of the mahogany plant (*Swietenia macrophylla*). The distributions of several physiologically relevant ions on a virtual section through the sample have been determined. These distributions are of interest to plant physiologists who study the long range ion transport in plants. Using XFEMT the sample preparation for these plant samples was greatly relaxed as the difficult step of cryo sectioning the sample was not needed. Reducing the amount of required sample preparation further is one of the major goals of future development. Ultimately, the acquisition of *in vivo* fluorescence microtomograms is envisioned.

The combination of fluorescence detection and tomographic techniques have been previously investigated¹⁻³ with a focus on larger samples and with resolutions in the millimeter range. Only recently, with the availability of high intensity microbeams, high resolutions in the micron range have become feasible.⁴ Besides fluorescence microtomography, differential absorption contrast tomography is a powerful method for three dimensional elemental mapping.^{5,6} However, this method requires sufficiently large pixel sizes and high concentrations of the elements of interest and is complementary to the technique described.

In section 2 we briefly review compound refractive lenses and how they can be used to produce the high intensity microbeam required for fluorescence microtomography at the synchrotron. While the experimental setup is described in section 3, a simple model describing fluorescence microtomography is given in section 4. Reconstructions of various element distributions on a virtual section through the mahogany root are discussed in section 5.

2. HARD X-RAY MICROBEAMS PRODUCED BY PARABOLIC COMPOUND REFRACTIVE LENSES

Parabolic compound refractive lenses are high quality imaging optics for hard x-rays that work in analogy to glass lenses in visible light.^{7,8} Since the refractive index of hard x-rays in matter is only

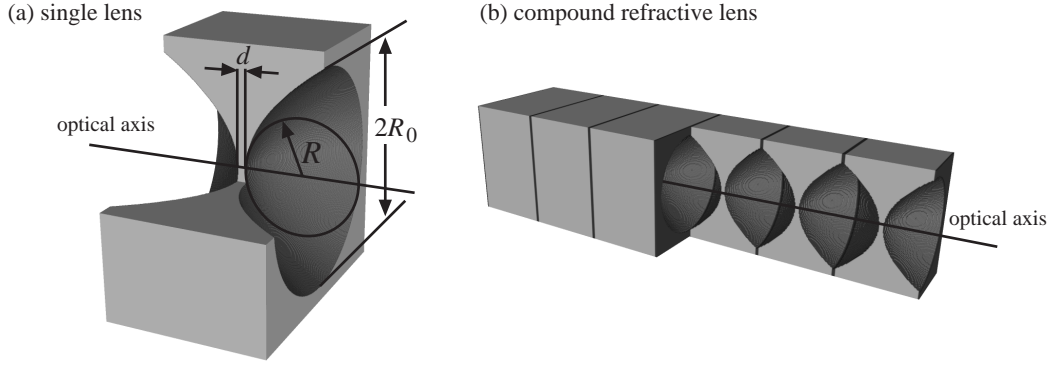


Figure 1. Parabolic compound refractive lens. (a) single lens. The refraction of a single lens is very weak, and many (N) lenses need to be stacked behind each other to form a compound refractive lens (b) in order to achieve a focal distance in the range of 1m and below.

slightly smaller than one ($n = 1 - \delta + i\beta$, $\delta \sim 10^{-6}$), refractive focusing optics have to have concave shape (see Fig. 1(a)). The very weak refraction requires both strong curvature of the individual lens surfaces (radius of curvature $R = 200\mu\text{m}$) and the stacking of many N individual lenses behind each other to obtain a focal distance $f = R/2N\delta$ of a meter or below (see Figure 1(b)). Since absorption inside the lens is significant for all lens materials, the choice of the lens material as well as the minimization of the thickness d of the lenses is important (Fig. 1(a)). To minimize absorption low Z lens materials should be used, such as beryllium, boron, carbon, or aluminium.^{9,10} The parabolic shape of the lens surfaces corrects for spherical aberration.⁸

Increasing absorption in the outer parts of the lens leads to an effective aperture D_{eff} that is smaller than the geometric aperture $2R_0$.⁸ Together with the focal distance f the effective aperture D_{eff} determines the optical properties such as the lateral resolution and the depth of field. Details about the dependence of the effective aperture on absorption and lens surface roughness can be found in Lengeler *et al.*⁸

To produce a high intensity hard x-ray microbeam, a third generation undulator source can be imaged onto the sample in a strongly demagnifying geometry. This is achieved by placing the lens into the monochromatic* synchrotron beam at a large distance L_1 from the source. The sharp image of the source is produced a distance $L_2 = \frac{L_1 f}{L_1 - f}$ behind the lens at the sample position. The lateral extension of the microbeam is determined by the source size, the magnification $m = L_2/L_1$ of the setup, and the diffraction broadening at the lens' effective aperture D_{eff} .⁸

For the fluorescence microtomography experiment described in this article, the monochromatic x-rays (19.5keV) of the undulator source at beamline ID18 of the European Synchrotron Radiation Facility (ESRF) in Grenoble, France, was focussed onto the sample by an aluminium compound refractive lens ($N = 150$, $R = 200\mu\text{m}$, $f = 45\text{cm}$, $L_1 = 58\text{m}$, $L_2 = 46\text{cm}$). The lateral beam size measured by a fluorescence knife edge technique was $1.4\mu\text{m}$ full width half maximum (FWHM) vertically and $6\mu\text{m}$ FWHM horizontally. Using a PIN-diode between the lens and the sample (see Fig. 2), the flux in the microbeam was measured to be above 10^{10}ph/s during the whole

*The undulator radiation is monochromatized by a Si-111 double crystal monochromator.

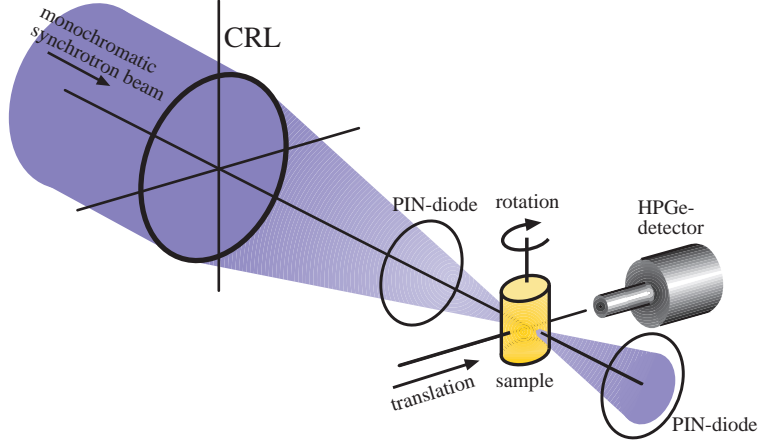


Figure 2. Schematic sketch of the x-ray fluorescence element microtomography (XFEMT) setup. The monochromatic x-rays from the undulator source are focused onto the sample. The PIN-diode between lens and sample measures the incident flux, while the second PIN-diode behind the sample records the radiation transmitted through the sample. The sample is scanned through the microbeam in both translation and rotation as depicted. The fluorescence radiation emanating from the sample is recorded at each step by the HPGe-detector.

experiment. The transmission through the sample was measured by a second PIN-diode placed behind the sample.

For a microbeam experiment, the depth of field is given by

$$d_{\text{long}} = 4 \frac{b_v / (2\sqrt{2 \ln 2}) \cdot L_2}{D_{\text{eff}}}, \quad (1)$$

where b_v is the FWHM beam size in the vertical direction. The particular microbeam above has a depth of field of $d_{\text{long}} = 10.8\text{mm}$. For samples that are smaller than the depth of field, the microbeam can be considered to have constant lateral extensions. This is true for the mahogany root considered in this article, whose diameter is smaller than 1mm.

3. FLUORESCENCE MICROTOMOGRAPHY

To record a fluorescence microtomogram the sample is scanned through the microbeam in horizontal translation perpendicular to the incident microbeam as shown in Fig. 2. At each scanning step the fluorescence radiation emanating from the sample is recorded by an energy dispersive detector. Taking advantage of the polarization of the undulator radiation, the detector is placed to face the sample perpendicularly to the incident beam in the horizontal plane, thus minimizing elastic and inelastic scattering into the detector. When the horizontal scan is completed, the sample is rotated by an integer fraction of the full circle and the horizontal scan is repeated. The whole procedure is continued until the sample has completed a full rotation.

To assess the applicability of XFEMT to biological samples, we have investigated several freeze dried plant samples. As an example, the results obtained for a root of the mahogany plant are shown

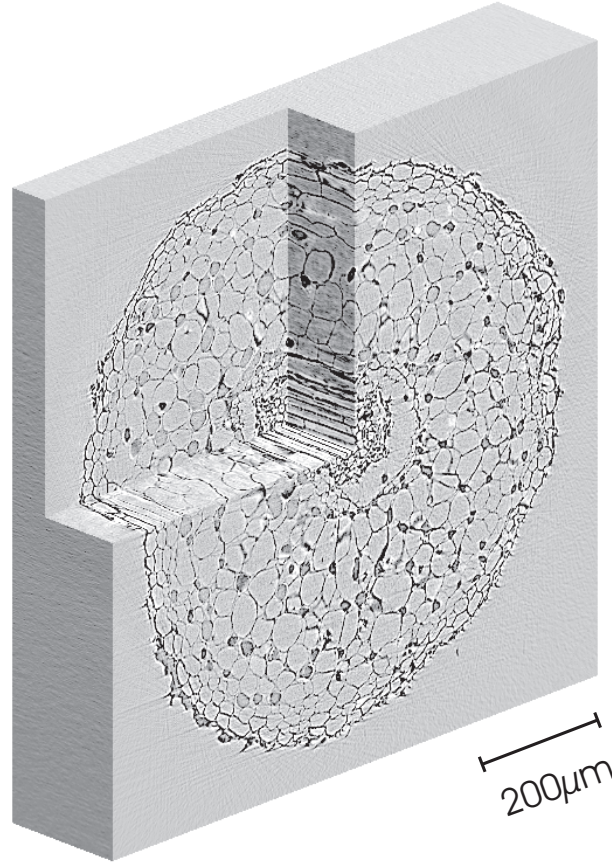


Figure 3. Phase contrast microtomogram of a root of the mahogany plant (*Swietenia macrophylla*). The three-dimensional reconstruction can be used to relate the element distribution obtained by XFEMT to the structure of the root.

in this article. In order to relate the distribution of several physiologically relevant elements to the structure of the root, we have recorded a phase contrast microtomogram of the sample. The reconstruction of the root is shown in Figure 3. It was recorded at the tomography station¹¹ of beamline ID22 of the ESRF at 20keV. 1250 projections over 180° were recorded using the FReLoN2000 high resolution CCD camera. The effective pixel size was 1.4 μ m and the object to camera distance was 50mm. For the reconstruction filtered backprojection was used.

The fluorescence microtomogram of the root of the mahogany plant was recorded scanning the sample through the microbeam in 128 steps with a step size of 6 μ m. This step size was adjusted to the FWHM size of the microbeam. This step size was chosen to minimize the total acquisition time at the expense of a slight undersampling. 151 horizontal scans (projections) each rotated by 2.38° with respect to the previous one were recorded over 360°. The fluorescence radiation for chlorine, potassium, calcium, iron, and rubidium were simultaneously measured (acquisition time 1s) at each step together with the inelastic (Compton) and elastic (Rayleigh) radiation. A high purity germanium detector with a 7mm² aperture was positioned about 18mm from the microbeam. Its energy resolution at Mn K α was measured to 170eV. The data for the potassium K α and the Compton scattering radiation are shown in the sinograms in Fig. 4.

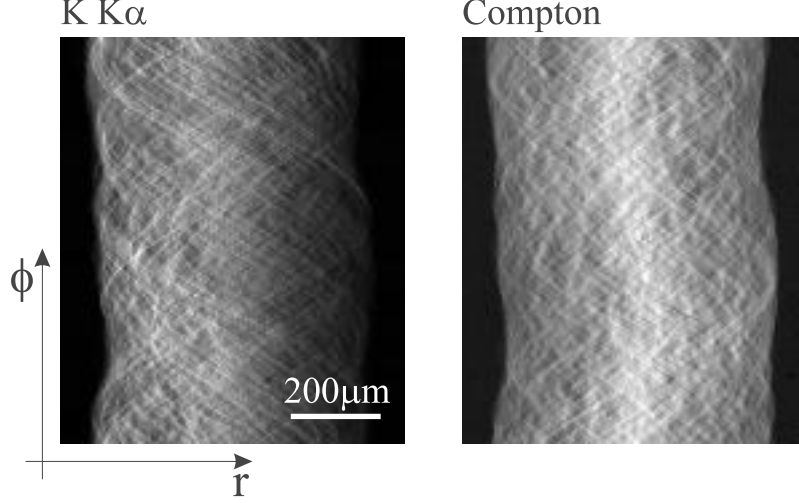


Figure 4. Sinograms for the potassium $K\alpha$ and the Compton scattering radiation. The potassium $K\alpha$ and Compton intensity is plotted in shades of gray as a function of the translational scanning position r (horizontal axis) and the rotation angle ϕ (vertical axis).

4. MODELING FLUORESCENCE MICROTOMOGRAPHY

In a simple model, the incident microbeam excites fluorescence radiation inside the sample along its path as shown in Fig. 5. The position of the microbeam with respect to the sample is given by the coordinate r in the (s, r) coordinate system. The origin of this coordinate system coincides with that of the (x, y) coordinate system that is fixed with respect to the sample and follows the rotation of the sample by ϕ . Neglecting all influences of absorption inside the sample, the detector signal is given by the line integral of the fluorescence coefficient $p(x, y)$ of the element under consideration

$$I(r, \phi) = I_0 \frac{\Omega}{4\pi} \cdot \int ds p(x(s, r), y(s, r)) \quad (2)$$

where

$$p(x, y) = c(E_1, \text{element}) \cdot \rho(x, y) \quad (3)$$

is proportional to the density ρ of the element. The proportionality factor c takes into account the photo absorption, fluorescence yield and the branching factor for the given element at the incident photon energy E_1 . Ω is the solid angle spanned by the detector and is assumed to be constant for all positions s inside the sample.

By neglecting absorption effects (2) is the simple Radon transform of p , and $p(x, y)$ can be found using standard tomographic reconstruction techniques, such as filtered backprojection. In general, however, the incident microbeam as well as the fluorescence radiation are attenuated inside the sample. These two effects call for modifications of (2)¹⁻³:

$$I(r, \phi) = I_0 \cdot \int ds f(\phi, s, r) \cdot p(x(s, r), y(s, r)) \cdot g(\phi, s, r), \quad (4)$$

where

$$f(\phi, s, r) = \exp\left(-\int_{-\infty}^s ds' \mu_1(s', r)\right) \quad (5)$$

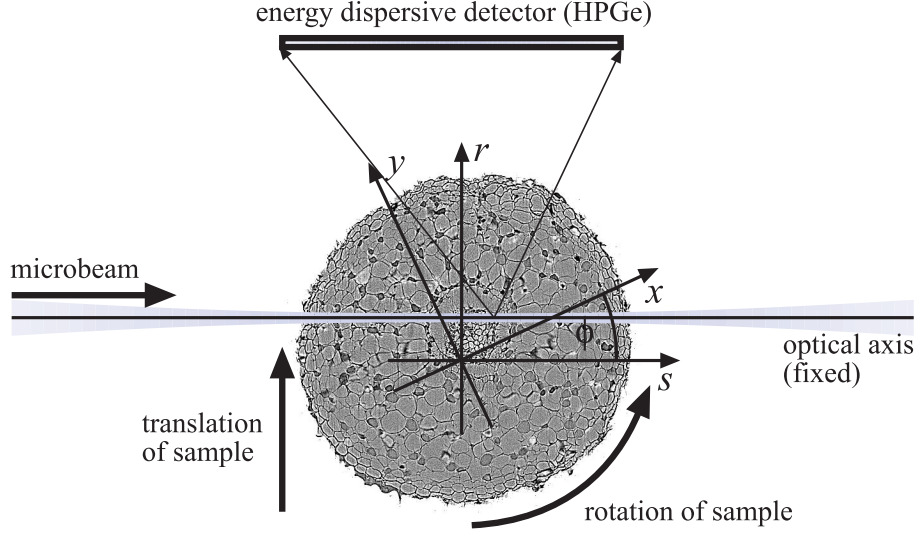


Figure 5. Modeling fluorescence microtomography.

accounts for the absorption of the incident beam up to the point (s, r) , and

$$g(\phi, s, r) = \frac{1}{4\pi} \int_{\Omega} d^2\gamma \exp\left(-\int_{G(\gamma, \phi, s, r)} dg \mu_F(x, y, z)\right) \quad (6)$$

determines what fraction of the fluorescence radiation produced at the point (s, r) reaches the detector. $\mu_I(x, y)$ and $\mu_F(x, y, z)$ are the attenuation coefficient distributions inside the sample at the incident and fluorescence energy, respectively. For each direction γ inside the solid angle Ω spanned by the detector, the attenuation along the straight path $G(\gamma, \phi, s, r)$ from the point (s, r) pointing towards the detector in the direction γ is integrated in (6). Multiple scattering effects are neglected. They might have to be taken into account when quantitative reconstruction is aimed for.¹² The tomographic problem (4) is by far more complicated than the inverse Radon problem (2) even when $\mu_I(x, y)$ and $\mu_F(x, y, z)$ are known. A simple inversion formula is not known. However, the implementation of numerical inversion methods, such as ART like methods,³ singular value decomposition,² or a conjugate gradient approach, is straight forward.

The attenuation coefficient distributions $\mu_I(x, y)$ for the incident radiation and $\mu_F(x, y, z)$ for the fluorescence radiation are a priori unknown. $\mu_I(x, y)$ can be reconstructed from the transmission data collected by the second PIN-diode behind the sample, but $\mu_F(x, y, z)$ is specific for each fluorescence line recorded and is not directly accessible by the experiment. For example Yuasa *et al.*² have suggested to record a transmission tomogram for each fluorescence line to obtain access to $\mu_F(x, y, z)$, but this is not a very practical approach if many fluorescence lines are investigated. To avoid this difficulty (and similar to approaches in single photon emission spectroscopy¹³) we have developed a self-consistent method to estimate $\mu_F(x, y, z)$ from the measured sinograms. Details of this method are beyond the scope of this article and will be published elsewhere.¹⁴

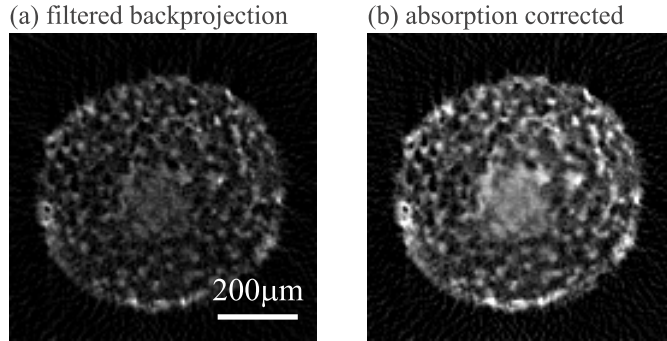


Figure 6. (a) reconstruction of the potassium distribution inside the mahogany root using filtered backprojection without taking absorption effects into account. (b) reconstruction of the potassium distribution correcting for selfabsorption inside the plant.

5. ELEMENT DISTRIBUTION INSIDE THE ROOT OF *SWIETENIA MACROPHYLLA*

As measured by the second PIN-diode behind the sample (Fig. 2) the mahogany root sample is practically transparent for the incident radiation ($E_1 = 19.5\text{keV}$). Therefore, $f(\phi, s, r) = 1$ to very good approximation and may be neglected in (4). $g(\phi, s, r)$ on the other hand, is not negligible for the fluorescence radiation of some of the elements, as can be seen in the sinogram in Fig. 4. The potassium $K\alpha$ signal for example is weaker on the right side of the sinogram that corresponds to the far side of the detector than on the left side that faces the detector. This is due to absorption of the $K K\alpha$ radiation inside the sample. Without absorption the sinogram would be symmetrical. Ignoring the absorption and using filtered backprojection to reconstruct the potassium distribution from the sinogram in Fig. 4 yields the distribution shown in Fig. 6(a). Fig. 6(b) shows the reconstruction of the potassium distribution taking absorption effects into account. Comparison of both reconstructions shows that filtered backprojection generally underestimates the concentrations. In addition, the distribution is distorted, particularly underestimating the concentrations in the center of the root, which are most effectively shielded.

For the Compton signal (18.7keV), on the other hand, the sinogram is symmetric and no attenuation toward the far side of the detector is observed. $g(\phi, s, r)$ can therefore be neglected and standard filtered backprojection may be used to reconstruct the sources of the Compton signal inside the sample.

Figure 7 shows the absorption corrected reconstructions of the distributions for chlorine, potassium, calcium, rubidium, and those of the sources of Compton and Rayleigh scattering[†]. A comparison with the phase contrast microtomogram shown in Fig. 3 shows that high concentrations of chlorine, potassium and rubidium can be found in the smaller, darker cells, while high concentrations of calcium are found on the surface of the root. The calcium distribution inside the plant can be barely resolved from the noise. To obtain a clearer picture of the calcium distribution inside the plant, the dynamic range of the reconstruction needs to be increased by increasing the count rate.

[†]The Compton and Rayleigh scattering signals can be used to map the distribution of an effective atomic number Z of the matrix¹⁵

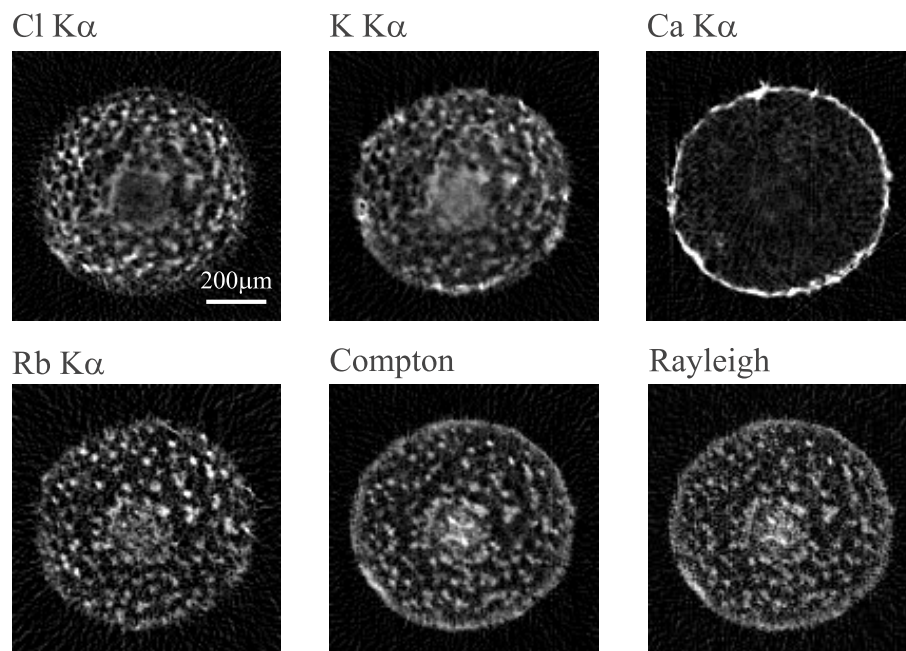


Figure 7. Reconstruction of the distributions of several physiologically relevant ions inside the root of the mahogany plant (*Swietenia macrophylla*). The Compton and Rayleigh scattering sources were reconstructed, as-well.

This can be achieved for example by increasing the acquisition time. The rubidium concentration is about 0.003 times smaller than that of potassium ($\sim 100\text{mmol/l}$ in maxima), illustrating the low detection limits that can be obtained by exciting the fluorescence by monochromatic x-rays. The acquisition time for each point in the scan was 1s.

6. CONCLUSION

X-ray fluorescence element microtomography (XFEMT) can be used to determine the distribution of elements inside a sample with minimal sample preparation. Which elements can be mapped depends on the absorption inside the sample. So far, for plant samples such as the mahogany root considered above, elements down to phosphorus could be detected in air, and reconstructions with sufficient dynamic range were obtained for chlorine and higher Z elements. Due to the excitation with monochromatic x-rays, the detection limits are low, allowing to determine the distribution of dilute elements. The resolution is limited by the horizontal step size, which itself is limited by the size of the microbeam and the sample. To obtain quantitative results in the future, more elaborate modeling of the physical processes will be required, taking multiple scattering effects into account.¹²

ACKNOWLEDGMENTS

The *Swietenia macrophylla* samples were provided by G. Noldt, Ordinariat für Holzbiologie, University of Hamburg, Germany. The authors would like to thank H. Schlösser from the machine shop of the II. Physikalisches Institut of the University of Technology in Aachen for his excellent work in machining the high precision parts and tools required to fabricate the compound refractive lenses.

REFERENCES

1. J. P. Hogan, R. A. Gonsalves, and A. S. Krieger, "Fluorescent computer tomography: A model for correction of x-ray absorption," *IEEE Transactions on Nuclear Science* **38**(6), pp. 1721–1727, 1991.
2. T. Yuasa, M. Akiba, T. Takeda, M. Kazama, A. Hoshino, Y. Watanabe, K. Hyodo, F. A. Dilmanian, T. Akatsuka, and Y. Itai, "Reconstruction method for fluorescent x-ray computed tomography by least-squares method using singular value decomposition," *IEEE Transactions on Nuclear Science* **44**(1), pp. 54–62, 1997.
3. G.-F. Rust and J. Weigelt, "X-ray fluorescent computer tomography with synchrotron radiation," *IEEE Transactions on Nuclear Science* **45**(1), pp. 75–88, 1998.
4. A. Simionovici, M. Chukalina, M. Drakopoulos, I. Snigireva, A. Snigirev, C. Schroer, B. Lengeler, K. Janssens, and F. Adams, "X-ray fluorescence microtomography: experiment and reconstruction," in *Developments in X-ray Tomography II*, U. Bonse, ed., vol. 3772 of *Proceedings of the SPIE*, pp. 328–337, 1999.
5. U. Bonse, H. Johnson, M. Nichols, R. Nußhardt, S. Krasnicki, and J. Kinney, "High resolution tomography with chemical specificity," *Nuclear Instruments and Methods* **A246**, pp. 644–648, 1986.
6. U. Bonse, R. Nußhardt, F. Busch, R. Pahl, Q. C. Johnson, J. H. Kinney, R. A. Saroyan, and M. C. Nichols, "Optimization of CCD-based energy-modulated x-ray microtomography," *Rev. Sci. Instrum.* **60**(7), pp. 2478–2481, 1989.
7. B. Lengeler, C. G. Schroer, M. Richwin, J. Tümmler, M. Drakopoulos, A. Snigirev, and I. Snigireva, "A microscope for hard x-rays based on parabolic compound refractive lenses," *Applied Physics Letters* **74**(26), pp. 3924–3926, 1999.
8. B. Lengeler, C. Schroer, J. Tümmler, B. Benner, M. Richwin, A. Snigirev, I. Snigireva, and M. Drakopoulos, "Imaging by parabolic refractive lenses in the hard x-ray range," *J. Synchrotron Radiation* **6**, pp. 1153–1167, 1999.
9. B. Lengeler, J. Tümmler, A. Snigirev, I. Snigireva, and C. Raven, "Transmission and gain of singly and doubly focusing refractive x-ray lenses," *J. Applied Physics* **84**(11), pp. 5855–5861, 1998.
10. P. Elleaume, "Two-plane focusing of 30keV undulator radiation," *J. Synchrotron Rad.* **5**, pp. 1–5, 1998.
11. T. Weitkamp, C. Raven, and A. Snigirev, "An imaging and microtomography facility at the ESRF beamline ID 22," in *Developments in X-Ray Tomography II*, U. Bonse, ed., vol. 3772 of *Proceedings of the SPIE*, 1999.
12. L. Vincze, K. Janssens, B. Vekemans, and F. Adams, "Monte Carlo simulation of x-ray fluorescence and scattering tomography experiments," in *Developments in X-ray Tomography II*, U. Bonse, ed., vol. 3772 of *Proceedings of the SPIE*, pp. 328–337, 1999.
13. A. V. Bronnikov, "Approximate reconstruction of attenuation map in SPECT imaging," *IEEE Transactions on Nuclear Science* **42**(5), pp. 1483–1488, 1995.
14. C. G. Schroer, "Selfconsistent absorption correction for fluorescence microtomography," 2000. to be published.
15. P. Duvauchelle, G. Peix, and D. Babot, "Rayleigh to Compton ratio computed tomography using synchrotron radiation," in *Developments in X-ray Tomography II*, U. Bonse, ed., vol. 3772 of *Proceedings of the SPIE*, pp. 268–278, 1999.